Eco-Cooling Control Strategy for Automotive Air-Conditioning System: Design and Experimental Validation

Hao Wang, Mohammad Reza Amini, *Member, IEEE*, Qiuhao Hu, Ilya Kolmanovsky, *Fellow, IEEE*, and Jing Sun, *Fellow, IEEE*

***Abstract*— The operation of the air-conditioning (A/C) system can significantly increase the energy consumption of passenger vehicles. In this article, aiming at reducing the vehicle-level energy consumption in hot weather, an optimization-based energy-efficient control strategy for the A/C system, which is referred to as the eco-cooling, is developed and experimentally validated. The proposed eco-cooling strategy leverages the A/C system efficiency sensitivity to the vehicle speed and the thermal storage of the passenger cabin to coordinate the A/C operation with vehicle speed profile by actively shifting the A/C thermal load toward the more efficient region at higher vehicle speeds. The proposed strategy exploits model predictive control and incorporates speed preview information while enforcing constraints. The effectiveness of the control strategy is first demonstrated on a high-fidelity simulation model and then implemented experimentally on a hybrid electric vehicle. Repeatable vehicle tests show that, over a real-world city driving cycle, an average energy saving of 5.7% can be achieved at the vehicle level using the proposed eco-cooling strategy compared with a baseline A/C control strategy that runs A/C with a constant setting. This energy-saving is achieved, while the proposed eco-cooling strategy delivers a similar amount of cooling energy to the cabin compared with that of the baseline strategy with a 2.7% difference on average.**

***Index Terms*— A/C energy management, eco-cooling, hybrid electric vehicle (HEV), vehicle experiments.**

NOMENCLATURE

AFR	Air-fuel ratio (AFR) [−].
$\text{AFR}_{\text{stoich}}$	Stoichiometric AFR [−].
c_p	Specific heat capacity of air [J/(kg · K)].
E_{AC}	A/C system energy consumption [MJ].
E_{batt}	Battery capacity [MJ].
E_{comp}	Compressor energy consumption [MJ].
E_{DACE}	Discharge air-cooling energy [MJ].
E_{EDF}	EDF energy consumption [MJ].
E_{veh}	Vehicle energy consumption [MJ].
e_{avg}	Average speed tracking error [mph].
η_{sys}	Energy conversion efficiency [−].
λ	Equivalent AFR [−].
P_{aux}	A/C auxiliary power [W].
P_{comp}	A/C compressor power [W].
P_{DACP}	Discharge air-cooling power [W].
SOC	Battery state-of-charge [−].
σ_{err}	Standard deviation in speed tracking [mph].
T_{ain}	Vent air temperature [°C].
T_{amb}	Ambient air temperature [°C].
$T_{\text{amb}}^{\text{adj}}$	Adjusted ambient air temperature [°C].
T_{cab}	Cabin air temperature [°C].
$T_{\text{discharge}}$	Discharge air temperature [°C].
T_{evap}	Evaporator wall temperature [°C].
T_{int}	Cabin interior temperature [°C].
T_{shell}	Cabin shell temperature [°C].
T_{sp}	Cabin temperature set point [°C].
V_{veh}	Vehicle speed [mph].
$\dot{m}_{\text{bl}}$	Blower air flow rate [kg/sec].
A/C	Air conditioning.
CAL	Cabin air loop.
CAN	Controller area network.
CAV	Connected and automated vehicle.
DACE	Discharge air-cooling energy.
DACP	Discharge air-cooling power.
EDF	Electric ducted fan.
IPOPT	Interior Point OPTimizer.
iPTM	Integrated power and thermal management.
HEV	Hybrid electric vehicle.
HVAC	Heating, ventilation, and A/C.
MAF	Mass air flow.
MPC	Model predictive control.
LHV	Lower heating value.
LIN	Local interconnect network.
OEM	Original equipment manufacturer.
PWM	Pulsewidth modulation.
RL	Refrigerant loop.
SC03	Supplemental federal test procedure.
UDP	User datagram protocol.

Manuscript received February 5, 2020; revised August 9, 2020 and October 25, 2020; accepted November 12, 2020. Manuscript received in final form November 14, 2020. This work was supported by the United States Department of Energy (DOE) through the ARPA-E NEXTCAR Program under Award DE-AR0000797. Recommended by Associate Editor A. Vahidi. *(Corresponding author: Hao Wang.)*

Hao Wang, Mohammad Reza Amini, Qiuhao Hu, and Jing Sun are with the Department of Naval Architecture & Marine Engineering, University of Michigan, Ann Arbor, MI 48109 USA (e-mail: autowang@umich.edu; mamini@umich.edu; qhhu@umich.edu; jingsun@umich.edu).

Ilya Kolmanovsky is with the Department of Aerospace Engineering, University of Michigan, Ann Arbor, MI 48109 USA (e-mail: ilya@umich.edu).

Color versions of one or more figures in this article are available at https://doi.org/10.1109/TCST.2020.3038746.

Digital Object Identifier 10.1109/TCST.2020.3038746

I. Introduction

REDUCING fuel consumption and maintaining the desired thermal state for subsystems are the two major objectives of thermal management strategies for automotive systems. In extremely hot or cold weather conditions, the effectiveness of thermal management becomes more critical as it will also impact safety, emissions, and passenger comfort. Specific opportunities for energy-efficient thermal management have been identified for the combustion engine [1], [2], the electric machines [3], the battery [4]–[6], the aftertreatment system [7], and the HVAC system [8]–[11]. More recently, with the emergence of CAV technology [12]–[14], the iPTM has been considered in [15]–[17]. The iPTM strategy exploits vehicle speed preview and weather information to coordinate the power and thermal management systems to improve the vehicle-level energy efficiency.

Among all thermal subsystems in an electrified passenger vehicle, the A/C system represents the most significant auxiliary load for thermal management [18], [19]. The use of the A/C system, especially in extreme weather conditions, can dramatically increase the energy consumption of electrified vehicles [19], [20]. Fig. 1 illustrates the schematics of a typical A/C system for a vehicle with the electrified powertrain in which the onboard high-voltage battery pack supplies the power to the major power consumers in the A/C system, namely, the compressor (P_{comp}) and the other auxiliaries (P_{aux}), including the EDF for condenser and the blower. There are two major loops within the A/C system: the RL delineated by yellow lines and the CAL indicated by blue lines in Fig. 1. In practice, depending on the cooling power demand from the CAL, the actuators in the RL, including the compressor, the condenser fan, the thermal expansion valve, and so on, are coordinated to maintain the evaporator wall temperature (T_{evap}) within the desired and safe range. That is, the RL must be controlled to provide the desired cabin cooling while avoiding damage to the RL. The variables V_{veh}, T_{amb}, T_{shell}, $T_{\text{discharge}}$, T_{ain}, and $\dot{m}_{\text{bl}}$ shown in Fig. 1 represent the vehicle speed, ambient air temperature, cabin shell temperature, discharge air temperature, vent air temperature, and blower airflow rate, respectively. Note that $T_{\text{discharge}}$ can be different from T_{ain}, considering additional heat exchange along the cabin air delivery path.

A special characteristic of an automotive A/C system is the sensitivity of its efficiency to the vehicle speed. As the vehicle speed increases, the A/C system consumes less energy while providing the same cooling power to the cabin. This is dictated by the underlying physics, as the effective ram airspeed through the condenser increases as vehicle speed increases, and hence, the condenser dissipates the heat to the ambient faster, leading to higher efficiency of the A/C system. As demonstrated on a high-fidelity A/C system model, CoolSim,[1] the efficiency of the A/C system, in hot ambient (35 °C), increases by approximately 30% as the vehicle speed increases from 0 to 25 m/s [8]. The vehicle speed sensitivity of A/C system efficiency can be leveraged to coordinate the A/C operation with the vehicle speed changes to achieve vehicle level energy efficiency improvements. We refer to such a strategy as eco-cooling.

[1]The CoolSim model is developed by the National Renewable Energy Lab (NREL) [21].

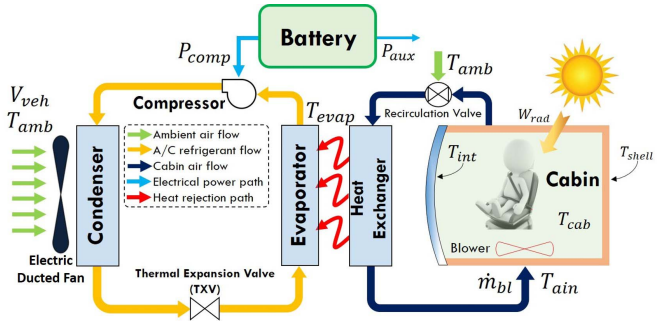

Fig. 1. Schematics of the electrified A/C system in an HEV. The electric battery power is used not only for part of traction power demand but also for auxiliary loads within the HEV, including that of A/C systems' actuators.

In this article, we consider an eco-cooling strategy that exploits MPC and vehicle speed preview while handling various system constraints. The proposed strategy is developed based on a physics-based A/C system model, which is referred to as the A/C simulation model hereafter. This model was previously presented in [22] and [23] for the vehicles with electrified powertrains. The energy-saving is then demonstrated in closed-loop simulations with the A/C simulation model while comparing the eco-cooling strategy with a production benchmark controller. A similar idea of leveraging A/C system efficiency to vehicle speed for energy saving has been reported in our previous works [8], [17] using different control strategies. In this article, to facilitate the implementation on a test vehicle and for consistency with the benchmark controller, a practical metric quantifying the A/C cooling performance, DACP, is incorporated into the design of the eco-cooling strategy. After validating its effectiveness on the A/C simulation model, the proposed eco-cooling strategy is implemented and tested on an experimental vehicle (Toyota Prius HEV MY 2017).

Compared with the demonstration of the proposed eco-cooling strategy on the simulation model, there are a number of challenges for demonstrating thermal management impact on the test vehicle, including the following.

1) The model mismatch between the simulation model and the physical system of the vehicle.
2) Uncertainties associated with the ambient thermal conditions (e.g., ambient temperature variation and cloud coverage) and powertrain control (e.g., power-split) in field tests. While, in the simulation environment, the power-split logic is known and can be tuned, such a strategy on the test vehicle is not known as its details are proprietary to OEMs.

These challenges need to be carefully considered and addressed in the vehicle testing in order to characterize the actual impact of the eco-cooling strategy. To this end, the test vehicle is instrumented to allow real-time control of the A/C system. A control-oriented model is developed for the A/C system and validated using the data collected from the test vehicle. The MPC-based eco-cooling strategy is developed,

which exploits the control-oriented model for prediction. The optimized trajectories of control inputs (blower airflow rate and cabin temperature set point) are computed for a real-world city driving cycle and applied to the test vehicle. By comparing with a conventional constant A/C control setting, vehicle-level energy saving is demonstrated with repeated vehicle tests over the same driving cycle. The overall cooling performance of applying the proposed eco-cooling strategy and the constant A/C setting is also compared using the cabin temperature trajectories and the DACE [23]. Note that, while a related eco-cooling strategy has been considered in our previous work [23], this article goes significantly beyond [23] in presenting the original experimental results and additional details and developments.

The rest of this article is organized as follows. In Section II, the eco-cooling strategy and its validation on the A/C simulation model are presented. The benefits of the eco-cooling strategy as observed in the simulations are characterized. In Section III, we present the modified eco-cooling strategy, which is suitable for vehicle implementation. The vehicle testing procedure is reported, and the repeatability of the road tests is discussed in Section IV followed by the test results and discussions in Section V. Summary and conclusions are presented in Section VI.

II. Eco-Cooling Strategy

A. Control-Oriented Modeling of the A/C Simulation Model

Physics-based modeling of the A/C system can be very challenging [24], especially for modeling the RL shown in Fig. 1. For initial development and evaluation of the eco-cooling strategy, we utilize the same simulation model, as previously presented in [22], [23]. General schematics of the A/C simulation model are illustrated in Fig. 2. This model simulates the entire A/C system for a passenger car and is integrated with the controller module that implements two levels of controls. A high-level controller is inside the climate control panel block, and it reflects the control settings (e.g., blower level and temperature set point) from the real vehicle, which directly affects the occupant's thermal comfort. Low-level controllers take the command from the control panel and regulate the behaviors of the physical system via the electric compressor control and the front end airflow control. The strategy for the low-level control of the compressor is proprietary to the vehicle manufacturer, which we do not have access to. The boundary conditions are set according to different simulation requirements (see [22] and [23] for more details about the A/C simulation model).

Similar to other high-fidelity A/C system models [24], the A/C simulation model involves detailed thermal and fluid dynamics of the refrigerant and has a large number of lookup tables containing calibration data, making it not amenable for controller design. Therefore, a simplified model of the system dynamics is necessary. In this work, the following discrete-time phenomenological model is used for prediction

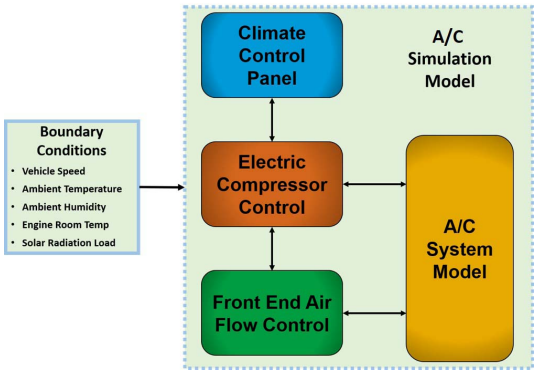

Fig. 2. Schematics of the A/C simulation model.

in the MPC design [23]:

$$\begin{aligned} T_{\text{evap}}(k+1) &= f_{T_{\text{evap}}}(k) = T_{\text{evap}}(k) \\ &\quad + \gamma_1\left(T_{\text{evap}}(k) - T_{\text{evap}}^{\text{targ}}(k)\right) \\ &\quad + \gamma_2(T_{\text{evap}}(k) - T_{\text{amb}})\dot{m}_{\text{bl}}(k) \\ &\quad + \gamma_3(T_{\text{evap}}(k) - T_{\text{amb}})\Delta\dot{m}_{\text{bl}}(k) + \gamma_4 \quad (1) \\ \dot{m}_{\text{bl}}(k+1) &= f_{\dot{m}_{\text{bl}}}(k) = \dot{m}_{\text{bl}}(k) + \Delta\dot{m}_{\text{bl}}(k) \quad (2) \\ T_{\text{discharge}}(k) &= f_{T_{\text{discharge}}}(k) \\ &= \gamma_5 T_{\text{evap}}(k) + \gamma_6 T_{\text{cab}}(k) + \gamma_7 \quad (3) \end{aligned}$$

where T_{cab}, T_{evap}, T_{amb}, $\dot{m}_{\text{bl}}$, and $T_{\text{discharge}}$ represent the cabin average air temperature, the evaporator wall temperature, the ambient temperature, the blower airflow rate, and the discharge air temperature, respectively. All temperatures are in °C, and the blower airflow rate has the unit of kg/s. The model states are T_{evap} and $\dot{m}_{\text{bl}}$. The model inputs are the incremental blower airflow rate, $\Delta\dot{m}_{\text{bl}}$, and the evaporator wall temperature target, $T_{\text{evap}}^{\text{targ}}$. The model parameters, γ_i $(i = 1, 2, \ldots, 7)$, are constants that are identified by matching the measured system response. This prediction model is nonlinear because of the multiplicative coupling between model states and inputs in (1).

Compared with the first-order evaporator wall temperature model proposed in [8] and [17], in which $T_{\text{evap}}^{\text{targ}}$ is an input, the model (1)–(3) reflects the airflow effects through both $\dot{m}_{\text{bl}}$ and $\Delta\dot{m}_{\text{bl}}$ terms. The incremental blower airflow ($\Delta\dot{m}_{\text{bl}}$) is treated as an input since it leads to better accuracy of the identified control-oriented prediction model. This model structure is consistent with the observation that with fixed $T_{\text{evap}}^{\text{targ}}$ and T_{evap} change when airflow changes.

To identify unknown parameters in (1)–(3), the A/C simulation model is simulated with different random sinusoidal input signals. The system responses are sampled every $T_s = 3$ s. Standard least-squares algorithm is applied to the simulated data, and the resulting identified parameters are $\gamma = [\gamma_1, \gamma_2, \ldots, \gamma_7] = [-0.084, -0.487, -1.121, -1.730, 0.729, 0.690, -11.457]$.

Fig. 3 shows the model (1)–(3) validation results on a different set of simulated data (not used for parameter identification). It demonstrates that the prediction model (1)–(3) matches the outputs of the high-fidelity A/C simulation model

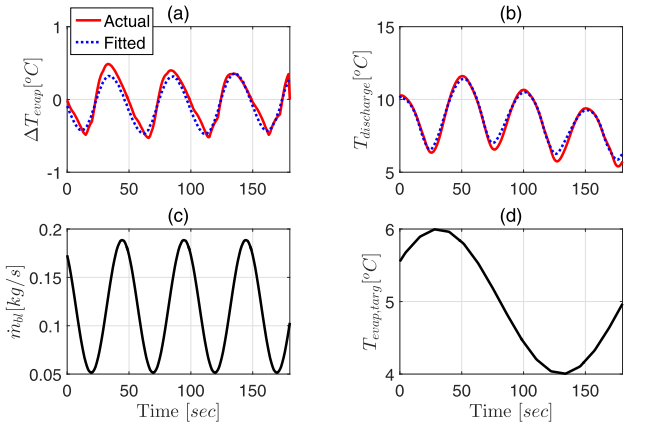

Fig. 3. Model validation results of (a) $\Delta T_{\text{evap}}(k) = T_{\text{evap}}(k+1) - T_{\text{evap}}(k)$ and (b) $T_{\text{discharge}}(k)$ for (c) and (d) given sinusoidal excitations to the A/C simulation model.

and confirms its acceptable accuracy in representing the key dynamics of the A/C system.

B. MPC-Based Eco-Cooling Strategy

To quantify A/C cooling performance and facilitate the controller design, a practical performance metric, DACP, is defined as follows:

$$P_{\text{DACP}}(k) = c_p(T_{\text{cab}}(k) - T_{\text{discharge}}(k))\dot{m}_{\text{bl}}(k) \tag{4}$$

where c_p is the specific heat capacity of air, and k is the index of the discrete sampling instants. Note that the DACP in (4) is defined for the case when A/C is running in the recirculation mode, which is also the condition for which the A/C simulation model has been simulated. If the fresh air mode is considered, T_{cab} should be replaced by T_{amb} (ambient temperature). The integral of DACP over time is referred to as the DACE, and it is denoted by E_{DACE}. The DACE will be used to quantify the overall cooling delivered to the cabin over a specified time window.

The eco-cooling strategy is the solution of an MPC defined based on the following cost function and constraints:

$$\begin{aligned}
&\min_{\substack{\Delta\dot{m}_{\text{bl}} \\ T_{\text{evap}}^{\text{targ}}}} \sum_{i=0}^{N_p} \left\{ (P_{\text{DACP}}(i|k) - \beta(i|k) \cdot P_{\text{DACP}}^{\text{targ}}(i|k))^2 \right\} \\
&\text{s.t. } T_{\text{evap}}(i+1|k) = f_{T_{\text{evap}}}(i|k) \\
&\quad \dot{m}_{\text{bl}}(i+1|k) = f_{\dot{m}_{\text{bl}}}(i|k) \\
&\quad T_{\text{evap}}^{\text{LB}} \le T_{\text{evap}}(i|k) \le T_{\text{evap}}^{\text{UB}}(i|k) \\
&\quad 0.05 \text{ kg/s} \le \dot{m}_{\text{bl}}(i|k) \le 0.15 \text{ kg/s} \\
&\quad -0.05 \text{ kg/s} \le \Delta\dot{m}_{\text{bl}}(i|k) \le 0.05 \text{ kg/s} \\
&\quad 2\ ^\circ\text{C} \le T_{\text{evap}}^{\text{targ}}(i|k) \le 10\ ^\circ\text{C} \\
&\quad T_{\text{evap}}(0|k) = T_{\text{evap}}(k), \quad \dot{m}_{\text{bl}}(0|k) = \dot{m}_{\text{bl}}(k).
\end{aligned} \tag{5}$$

In (5), $x(i|k)$ designates the predicted values of x at the time instant $(k+i)\cdot T_s$ when the prediction is made at the time instant $k \cdot T_s$, while $f_{T_{\text{evap}}}$ is determined based on (1) [and later on (6)]. In the cost function, $P_{\text{DACP}}(i|k) = c_p(T_{\text{cab}}(i|k) - T_{\text{ain}}(i|k))\dot{m}_{\text{bl}}(i|k)$ can be inferred from (4), and

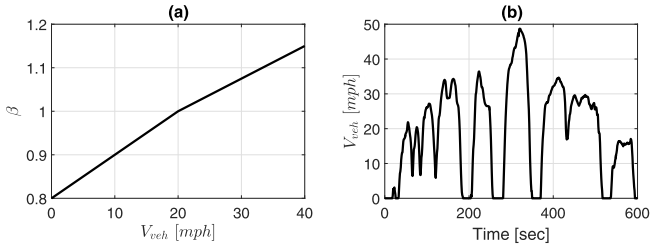

Fig. 4. (a) Speed-dependent β. (b) SC03 driving cycle.

$\beta(k)$ is a design parameter. $P_{\text{DACP}}^{\text{targ}}$ represents the target cooling trajectory that is the same as in the benchmark case for the nominal controller of the A/C simulation model. The main idea of the proposed eco-cooling strategy is to leverage the sensitivity of the A/C system efficiency to vehicle speed by the design of the speed-dependent β. Fig. 4(a) illustrates the dependence of β on the vehicle speed, V_{veh}. The increase in β as a function of V_{veh} promotes shifting the A/C thermal load to the more efficient region at higher vehicle speeds. The β values at different vehicle speeds are tuned by trial-and-error to provide the same E_{DACE} as the benchmark controller based on the simulation results for supplemental federal test procedure (SC03) driving cycle.

1) *Remark:* β could be treated as an extra optimization variable to tune eco-cooling strategy performance subject to target DACE over a specified driving cycle.

In (5), $T_{\text{evap}}^{\text{UB}}$ represents the time-varying upper bound for T_{evap}, the values of which are assumed to be specified over the prediction horizon. The design of time-varying $T_{\text{evap}}^{\text{UB}}$ is to emulate the initial cool-down operation for the automotive A/C system, which refers to the performance of the benchmark controller. $T_{\text{evap}}^{\text{LB}}$ is set to be a small positive constant to avoid evaporator from freezing. Time-independent constraints for other variables are imposed based on the system operating requirements.

C. Simulation Results

To evaluate the performance of the MPC-based eco-cooling strategy (5), the prediction horizon, N_p, is set to be 10, i.e., we are predicting ten steps ahead, which is 30 s considering the sampling time $T_s = 3$ s. The NMPC problem (5) is solved numerically using the MPCTools package [25]. This package exploits CasADi [26] for automatic differentiation and IPOPT algorithm for the numerical optimization.

The eco-cooling strategy is tested in a closed-loop with the A/C simulation model. Fig. 5 illustrates the implementation in Simulink. The MPC-based eco-cooling strategy updates the control inputs every 3 s, while the outputs from the A/C simulation model is sampled at 0.1 s. Thus, a data sampling block, as shown in Fig. 5, is incorporated in the feedback loop to match the MPC update rate with the feedback signal. Fig. 6 compares the simulation results of applying the eco-cooling strategy and an OEM benchmark controller. As shown in Fig. 6, the MPC-based eco-cooling strategy enforces the imposed state and input constraints that are plotted by red dotted lines, reasonably well. In Fig. 6(a), the violations of the

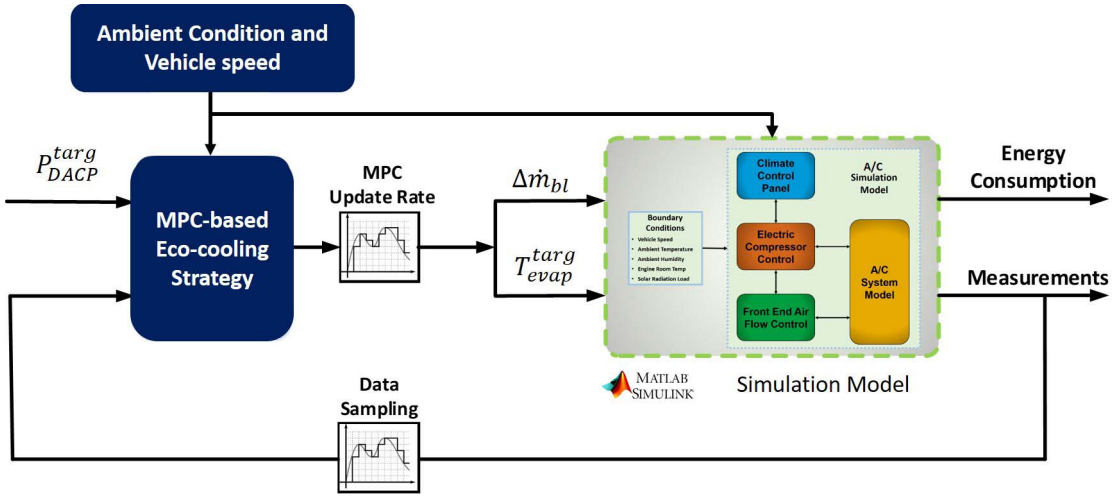

Fig. 5. Schematics of integrating the MPC-based eco-cooling with A/C simulation model in Simulink.

TABLE I
A/C SYSTEM ENERGY CONSUMPTION COMPARISONS BETWEEN THE BENCHMARK CASE AND THE ECO-COOLING STRATEGY

	E_{DACE} [MJ]	E_{comp} [MJ]	E_{EDF} [MJ]	E_{AC} [MJ]
Benchmark	1.378	0.689	0.104	0.793
Eco-cooling	1.392 (+1.0%)	0.647	0.101	0.748 (-5.7%)

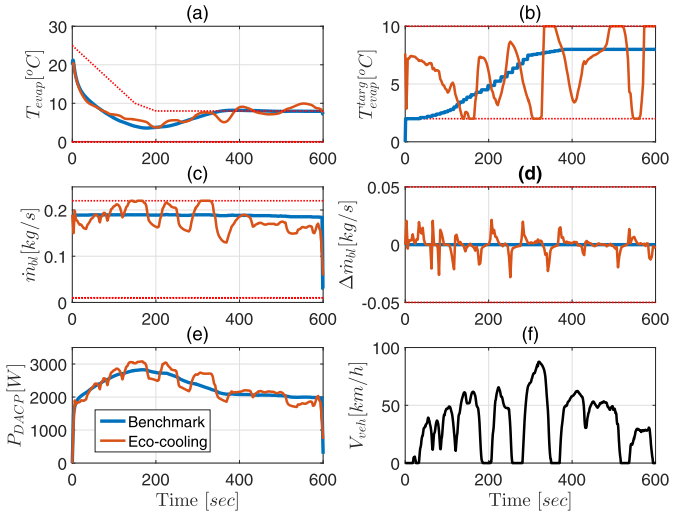

Fig. 6. Comparison between the proposed eco-cooling strategy and the benchmark controller in simulations using the A/C simulation model as the virtual testbed. Constraints are shown by red dotted lines.

upper bound of the evaporator temperature toward the end of the driving cycle are mainly due to the mismatch between the control-oriented model and the simulation model. It is noted that further improvements in model structure and controller fine-tuning could reduce the model mismatch. The control inputs are plotted in Fig. 6(b) and (d). Fig. 6(c) shows the airflow rate that is considered as a state in the optimization problem (5). As shown in Fig. 6(e), the eco-cooling strategy manipulates P_{DACP} as intended according to the vehicle speed [see Fig. 6(f)] to improve the energy efficiency.

Fig. 7 provides the comparison between the eco-cooling case and the benchmark case based on the time histories of the A/C power trajectories and additional temperature measurements. In addition, the energy consumption comparison for both cases over the SC03 driving cycle is summarized in Table I. DACE (E_{DACE}), compressor energy consumption (E_{comp}), and EDF energy consumption (E_{EDF}) are the time integral of their power traces, P_{DACP}, P_{comp}, and P_{EDF}, respectively. Compared with the benchmark case, the total A/C energy consumption ($E_{\mathrm{AC}} = E_{\mathrm{comp}} + E_{\mathrm{EDF}}$) is reduced by 5.7% for the eco-cooling case while providing 1% more cooling to the cabin in terms of E_{DACE}. Fig. 7(c) shows that, by introducing eco-cooling, the resulting cabin temperature is very close to that of the benchmark case, implying a small impact on passenger comfort. Finally, Fig. 7(d) shows the comparison of the discharge air temperature, which indicates that the deviation in the discharge air temperature is bounded within a couple of degrees for the eco-cooling case.

III. MODIFIED ECO-COOLING STRATEGY FOR VEHICLE IMPLEMENTATION

Considering the mismatch between the A/C simulation model and the physical A/C system of the test vehicle, the originally developed eco-cooling strategy validated in simulations is modified to enable vehicle implementation. In particular, the control inputs are changed to match the configuration of the vehicle control system. In the rest of this section, the control-oriented model of the vehicle A/C system and the modified eco-cooling strategy are presented.

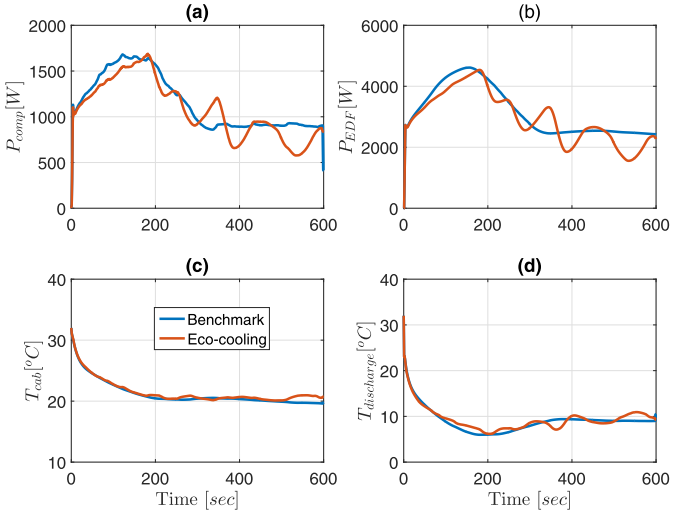

Fig. 7. Comparison between the proposed eco-cooling strategy and the benchmark controller in simulations on the A/C simulation model (A/C power trajectories and additional temperatures).

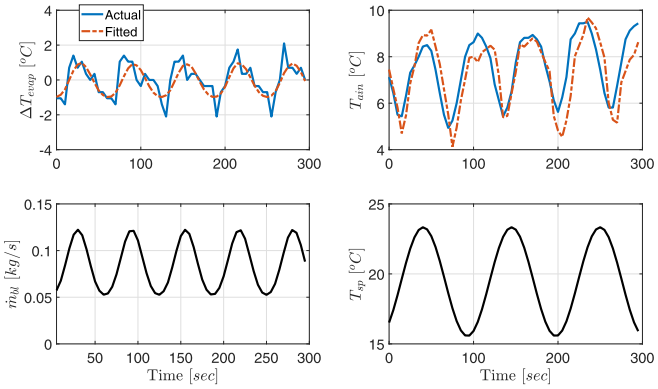

Fig. 8. Model validation results of $\Delta T_{\text{evap}}(k) = T_{\text{evap}}(k+1) - T_{\text{evap}}(k)$ and $T_{\text{ain}}(k)$ for the sinusoidal excitations applied to the A/C system on the test vehicle.

A. Control-Oriented Modeling of the Vehicle A/C System

Modifications to the prediction model (1)–(3) are made to account for the differences between the physical setup of the test vehicle and the A/C simulation model. Especially, in our test vehicle, the vapor-compression process (i.e., the operations of the compressor and the evaporator) is not directly controlled to avoid damaging A/C system components. Moreover, the target evaporator wall temperature ($T_{\text{evap}}^{\text{targ}}$) used as a control input on the A/C simulation model is not directly manipulated on the test vehicle. The implemented controller on the test vehicle manipulates the cabin cooling demand by adjusting the blower flow rate ($\dot{m}_{\text{bl}}$) and cabin temperature set point (T_{sp}). The control-oriented model for in-vehicle implementation of the MPC-based eco-cooling is defined as follows:

$$\begin{aligned} T_{\text{evap}}(k+1) &= f_{T_{\text{evap}}}(k) = \xi_1 T_{\text{evap}}(k) \\ &\quad + \xi_2 (T_{\text{ain}}(k) - T_{\text{amb}}) \dot{m}_{\text{bl}}(k) + \xi_3 \qquad (6) \\ T_{\text{ain}}(k) &= f_{T_{\text{ain}}}(k) \\ &= \xi_4 T_{\text{evap}}(k) + \xi_5 T_{\text{sp}}(k) \qquad (7) \end{aligned}$$

where T_{ain} represents the vent air temperature replacing $T_{\text{discharge}}$ in the original model (1)–(3) as $T_{\text{discharge}}$ is not measured in the test vehicle. The model state is T_{evap}. The model inputs are the blower airflow rate, $\dot{m}_{\text{bl}}$, and the cabin temperature set point (T_{sp}). The model parameters, ξ ($i = 1, 2, \ldots, 5$), are constants identified from the vehicle data. More details on the vehicle instrumentation are presented in Section IV-A. This model (6) is also nonlinear because of the multiplicative coupling between model state and input in (6). The model validation results are shown in Fig. 8 for the case when the sinusoidal input excitation is applied, while the vehicle is traveling on a local route in Ann Arbor, MI, USA. The sampling period is 5 s, and ξ ($i = 1, 2, \ldots, 5$) = $[1.0719, -1.2265, -2.8523, 0.8964, 0.1252]$ were identified using a different data set than used for validation. As shown in Fig. 8, the model can capture the evaporator wall temperature dynamics and match the vent air temperature reasonably well. This experimentally validated control-oriented model is used by the modified eco-cooling strategy.

B. Modified Eco-Cooling Strategy for Vehicle Implementation

The modified eco-cooling strategy is based on the control-oriented model [see (6) and (7)] and the following constrained optimization problem:

$$\begin{aligned} \min_{\substack{\dot{m}_{\text{bl}} \\ T_{\text{sp}}}} \ & \sum_{i=0}^{N_p} \left\{ (P_{\text{DACP}}(i|k) - \beta(i|k) \cdot P_{\text{DACP}}^{\text{targ}}(i|k))^2 \right\} \\ \text{s.t. } & T_{\text{evap}}(i+1|k) = f_{T_{\text{evap}}}(i|k) \\ & 0.5\ ^\circ\text{C} \le T_{\text{evap}}(i|k) \le 12^\circ\text{C} \\ & 0.05\ \text{kg/s} \le \dot{m}_{\text{bl}}(i|k) \le 0.13\ \text{kg/s} \\ & 16\ ^\circ\text{C} \le T_{\text{sp}}(i|k) \le 23\ ^\circ\text{C} \\ & T_{\text{evap}}(0|k) = T_{\text{evap}}(k). \qquad (8) \end{aligned}$$

This modified eco-cooling strategy (8) is, for the most part, similar to (5). In the cost function, $P_{\text{DACP}}(i|k) = c_p(T_{\text{amb}}(i|k) - T_{\text{ain}}(i|k))\dot{m}_{\text{bl}}(i|k)$, which reflects the vehicle test condition in fresh air mode. In previous simulations on the A/C simulation model, the recirculation mode was activated under high cooling load according to the benchmark control logic. $P_{\text{DACP}}^{\text{targ}}$ represents the target cooling trajectory that is the same as for the baseline controller (i.e., with the A/C system running when constant control inputs are applied). Fig. 9(a) shows the dependence of β with respect to the "Plymouth road driving cycle" shown in Fig. 9(b). This driving cycle was selected based on a real-world city vehicle speed profile for a six-intersection corridor at Plymouth Rd. in Ann Arbor [16], representing a congested city driving scenario. The same driving cycle is used for vehicle testing.

Fig. 10 shows the trajectories of the control inputs for the eco-cooling strategy when problem (8) is solved in closed-loop with the control-oriented model and compares them to constant cooling (benchmark) scenario. Note that, in Fig. 10, the units of the two control inputs, $\dot{m}_{\text{bl}}$ and T_{sp}, have been converted to percentage PWM control (%) and degrees Fahrenheit (°F), respectively, that correspond to the units of the actual control

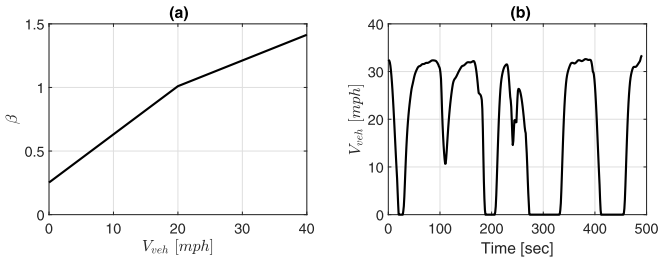

Fig. 9. (a) Speed-dependent β. (b) Driving cycle over Plymouth road in Ann Arbor.

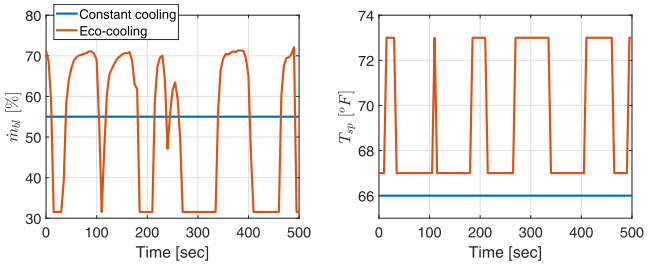

Fig. 10. Control inputs for the constant cooling and eco-cooling cases.

inputs in the vehicle A/C system. Note that T_{sp} is the temperature set point as input to the vehicle climate system, and it does not necessarily indicate any actual temperature measurements, considering that the airflow rate is also changing. These two sets of control inputs shown in Fig. 10 are tested on the vehicle to demonstrate the benefits of efficient A/C energy management. Direct implementation of MPC in the closed loop on the test vehicle requires extra hardware and software works, which are not trivial. Instead, in order to demonstrate the eco-cooling idea, we applied these off-line optimized controls shown in Fig. 10. Note that both cases provide the same DACE according to the simulation results on the control-oriented model.

Note that the optimization problem in (8) can be augmented with additional passenger comfort constraints [9]. For the vehicle demonstration in this article, such constraints are not considered for the sake of simplicity; we only focus on demonstrating the energy saving of the eco-cooling strategy.

IV. Vehicle Tests on Open Road

The primary objective of the road tests is to demonstrate the energy saving of the proposed eco-cooling strategy with respect to the more conventional constant cooling strategy. In order to characterize the impact of the energy-efficient cabin thermal management, the variability over different test trips needs to be reduced, especially for the powertrain traction loss and cabin boundary thermal conditions. To this end, the rest of this section presents the instrumentation of the test vehicle and discusses the testing procedures, which facilitated the repeatability of the tests.

A. Test Vehicle Instrumentation

Our test vehicle is a 2017 Toyota Prius Four Turing HEV. It has been instrumented in order to enable the

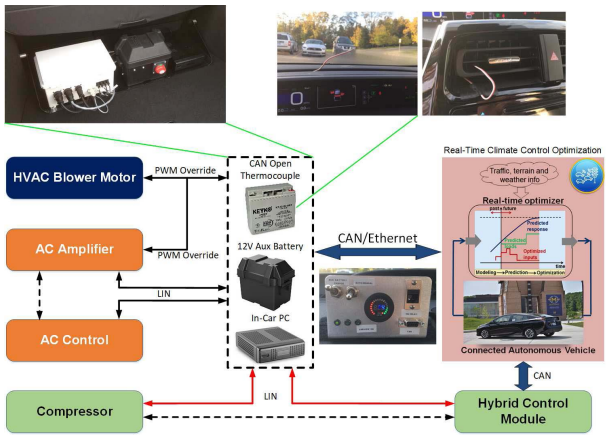

Fig. 11. Schematics of the modified Toyota Prius HVAC control system with added thermocouples, CAN open thermocouple module, auxiliary battery, and In-Car PC.

implementation of the HVAC controls and demonstrate the eco-cooling strategy performance. The schematics of the modified HVAC system are shown in Fig. 11.

As shown in Fig. 11, the original control loops are modified to access the available signals on the CAN and LIN buses through the In-Car PC via a NeoVI Fire module. The In-Car PC communicates with the testing laptop via Ethernet, where the CAN/LIN messages are read and logged through a LabVIEW interface. The LabVIEW interface allows for real-time data collection and intercepting the A/C control commands from the user. The commands, which can be sent to the vehicle in real time, include the blower flow rate, cabin temperature set point, blend door position set point, and AC ON/OFF command. In order to evaluate the thermal behavior inside the cabin, additional thermocouples have been installed within the cabin, and their signals have been added to the CAN bus. These thermocouples are shown on the top right of Fig. 11, including the temperature measured above the dashboard and at the vent outlet. During the vehicle test, the blend door position was fixed to the front vent where a thermocouple is mounted to measure the vent air temperature. Moreover, comprehensive airflow measurement tests have been performed to characterize the A/C air blower (see the Appendix for the map specifically used for the controller design in this work).

To facilitate the design and vehicle testing of the eco-cooling strategy, a Simulink interface was developed to parse the messages received from the CAN interface, which are used as feedback signals for the HVAC controller in real time. Moreover, the developed Simulink model sends the computed HVAC control signals to the vehicle by converting the control signals to UDP data. Overall, the instrumented vehicle allows us to log the vehicle data and update control commands by a Simulink-based controller interface.

B. Test Procedure and Vehicle Speed Tracking Performance

The road tests were performed on two different roads near Ann Arbor. The locations of the two test sites are shown in Figs. 12 and 13. Both testing routes are straight, with no stops, and very little traffic so that we can emulate the

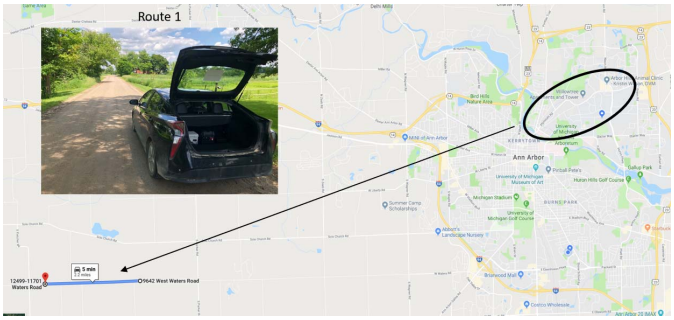

Fig. 12. Route 1 along W. Waters road with the Plymouth corridor [16] shown in the ellipse.

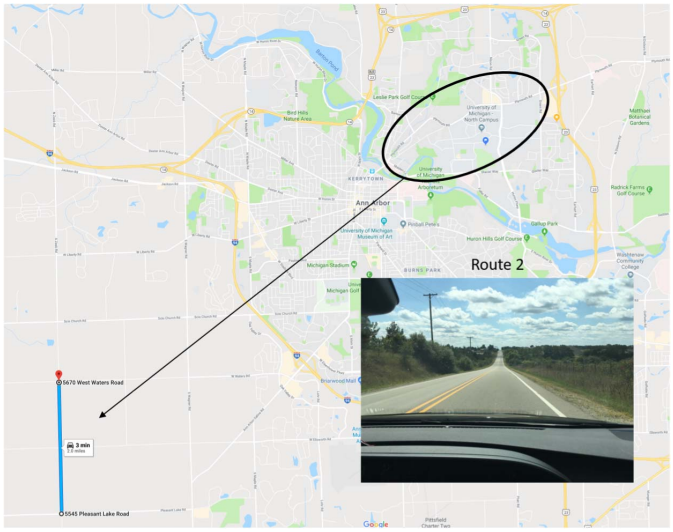

Fig. 13. Route 2 along S. Zeeb road with the Plymouth corridor [16] shown in the ellipse.

vehicle speed profile over the Plymouth road driving cycle shown in Fig. 9(b). In terms of the road conditions, Route 1 is mostly flat but unpaved, and Route 2 is paved but with larger deviations in road grade. The speed trajectory shown in Fig. 9(b) is tracked by a human driver.

For demonstrating the eco-cooling impact, 18 data sets were collected. A single data set consists of three consecutive trips on the same day following the Plymouth road driving cycle, with the first trip representing the calibration test followed by the constant cooling test and, finally, the eco-cooling test. All three tests started at the same location. Between two tests, the vehicle cabin was fully ventilated using the ambient air when driving back to the starting location. At the beginning of each test trip, the vehicle cabin temperature was controlled to be at 30°C. Note that the calibration test was utilized to prepare the test vehicle, and the data from the calibration test are not used for the energy consumption comparison.

The uncertainties associated with speed tracking by a human driver may affect vehicle energy consumption. In order to improve the speed tracking accuracy, a MATLAB/Simulink interface was created to guide the human driver. As shown in the bottom right of Fig. 14, both the current vehicle speed (in red dots) and the planned future speed (in blue line) are

Fig. 14. Vehicle test trip is ongoing along Route 1.

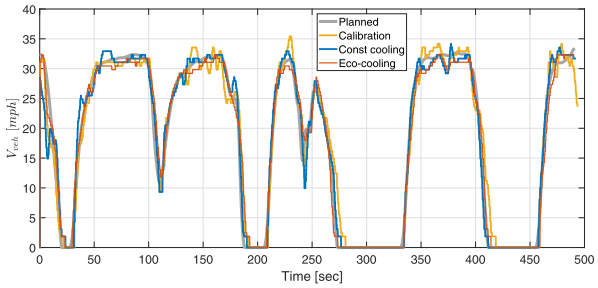

Fig. 15. Vehicle speed trajectories for the tests performed on May 31, 2019.

displayed on the testing laptop to help the driver follow the speed profile in real time.

Fig. 15 provides an example of the speed trajectories for the tests performed on May 31, 2019. As can be seen from the comparison with the planned Plymouth road driving cycle, the speed tracking error for all tests can be maintained within 2 mi for most of the time. In addition, the average speed tracking error (e_{avg}) and the standard deviation of the speed tracking error (σ_{err}) for each test are listed in Table II. Table II shows that the average speed tracking error of each test is negligible, while the standard deviation of the tracking errors is small and similar for constant cooling and eco-cooling cases. The tests with similar speed tracking results to this example are used to evaluate the energy consumption and cooling performance. In Fig. 16, the standard box plots illustrate the speed tracking performance in terms of e_{avg} (left) and σ_{err} (right) for all constant cooling and eco-cooling tests in 18 data sets. On each box, the central mark indicates the median, and the bottom and top edges of the box indicate the 25th and 75th percentiles, respectively. The whiskers extend to the most extreme data points not considered outliers, and the outliers are plotted individually using the "+" symbol. As shown in Fig. 16, the speed tracking error is well-controlled, and the overall tracking performance is similar for both cases.

V. Experimental Results

All the tests demonstrating the eco-cooling impact were performed over the time period between May 23 and September 5, 2019. The ambient air temperature (T_{amb}) during the testing period is varied within a large range between 22 °C to 34 °C depending on when the data were collected. In total,

TABLE II

AVERAGE SPEED TRACKING ERROR (e_{avg}) AND THE STANDARD DEVIATION OF THE SPEED TRACKING ERROR (σ_{err}) FOR THE TESTS PERFORMED ON MAY 31, 2019, AND SHOWN IN FIG. 15

	e_{avg} $[mph]$	σ_{err} $[mph]$
Calibration	0.24	2.52
Constant cooling	0.04	2.13
Eco-cooling	−0.11	1.98

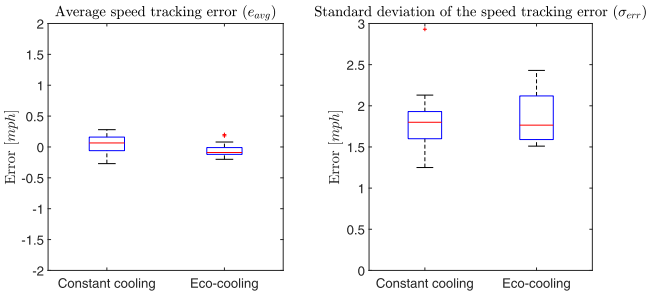

Fig. 16. Statistical evaluations of the speed tracking performance for all the eco-cooling tests.

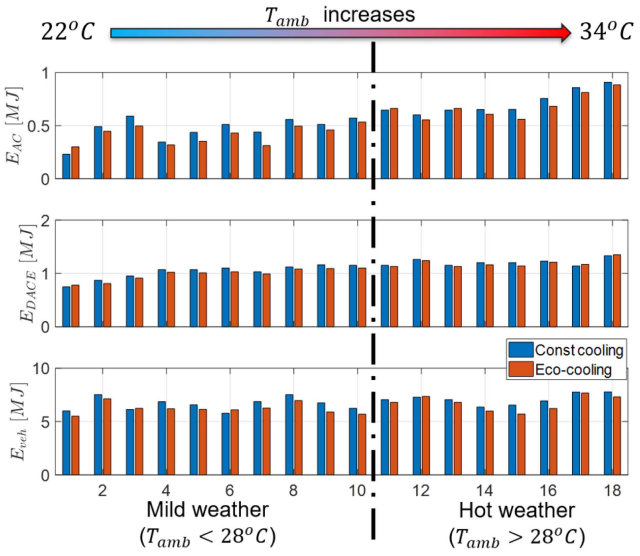

Fig. 17. Energy consumptions and cooling performance of each test with constant cooling and eco-cooling strategies.

18 data sets were collected (13 data sets were collected from the tests on Route 1, and five data sets were collected from the tests on Route 2). With well-controlled speed tracking performance, the average results of these 18 tests can characterize the benefits of the proposed eco-cooling strategy. Note that the vehicle-level energy consumption for each test trip is computed using the following equation:

$$E_{\text{veh}} = \int_0^{t_n} \frac{\dot{m}_{\text{air}}(t)}{\text{AFR}(t)} \cdot \text{LHV}\ dt + \frac{E_{\text{batt}} \cdot \Delta\text{SOC}}{\eta_{\text{sys}}} \tag{9}$$

$$\text{AFR}(t) = \lambda(t) \cdot \text{AFR}_{\text{stoich}} \tag{10}$$

$$\Delta\text{SOC} = \text{SOC}(0) - \text{SOC}(t_n) \tag{11}$$

where t_n represents the duration of each test run, $\dot{m}_{\text{air}}$ represents the airflow rate into the engine measured by the MAF sensor, AFR, λ, and $\text{AFR}_{\text{stoich}}$ represent the AFR, the equivalent AFR (measured), and the stoichiometric AFR, respectively, LHV represents the lower heating value of the gasoline, E_{batt} represents the battery capacity, η_{sys} represents the energy conversion efficiency from fuel energy to battery energy, and SOC represents the estimated battery state of charge from the measurement. The vehicle-level energy consumption (E_{veh}) computation is based on the adjusted fuel energy that accounts for the SOC deviation compared with its initial value [see (11)].

Fig. 17 reports the energy consumption and cooling performance in all tests resulted from constant cooling and eco-cooling strategies. The energy consumption is characterized by two metrics, E_{AC} and E_{veh}, that represent the A/C system energy consumption and vehicle-level energy consumption, respectively. The A/C system energy consumption is the integral of compressor power and blower power over time, which are directly measured in the test vehicle. Vehicle-level energy consumption is computed based on (9). In terms of the cooling performance, the DACE metric is used to quantify the overall cooling energy provided to the cabin over each trip. In our tests, DACE is calculated as follows:

$$E_{\text{DACE}} = \int_0^{t_n} c_p \cdot \left(T_{\text{amb}}^{\text{adj}}(t) - T_{\text{ain}}(t)\right) \cdot \dot{m}_{\text{bl}}(t)\ dt \tag{12}$$

where t_n is the duration of the trip, c_p is the specific heat capacity of air at constant pressure, and $T_{\text{amb}}^{\text{adj}}$ is the adjusted ambient temperature measurement, which represents the temperature of the air entering the A/C system (i.e., before exchanging heat with the evaporator). $T_{\text{amb}}^{\text{adj}}$ is often higher than the ambient air temperature (T_{amb}) considering extra heat picked up along the air path, where the heat energy mostly comes from the engine compartment. T_{ain} is the vent air temperature measured by the thermocouple located at the front vent, as shown in Fig. 11. $\dot{m}_{\text{bl}}$ is the blower airflow rate determined by the map shown in Fig. 20. In Fig. 17, all 18 tests are sorted by the ambient air temperature and are separated into two groups, corresponding to mild weather and corresponding to hot weather. As can be observed from Fig. 17, as the ambient air temperature increases, the A/C system energy consumption increases dramatically. More importantly, in most cases, the eco-cooling strategy saves energy from the A/C system, which can translate into vehicle-level energy saving. However, uncertainties associated with the road conditions, powertrain control, and weather conditions cannot be fully eliminated, leading to several outliers in the results.

A more clear comparison can be seen in Fig. 18, where average energy consumption and cooling performance are compared. Overall, the proposed eco-cooling strategy saves 8% of A/C system energy, which translates into 5.7% energy saving at the vehicle level. Although the average cooling performance in terms of E_{DACE} is slightly degraded by 2.7%, the analysis of energy savings at the A/C system level and vehicle level shows that these energy savings are still considerable and are not primarily due to DACE decrease. This energy-saving is achieved by leveraging the A/C system efficiency that depends on the vehicle speed. Comparing the results between

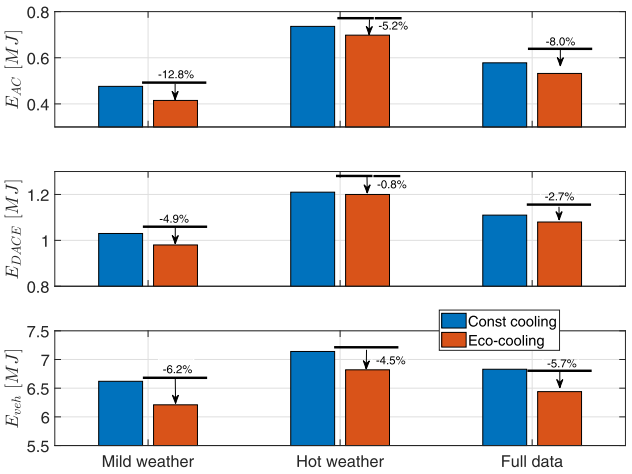

Fig. 18. Comparison of average energy consumption and cabin cooling results from constant cooling and eco-cooling strategies.

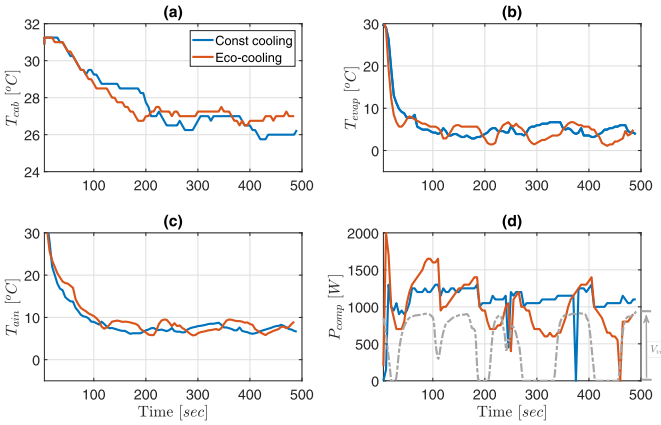

Fig. 19. Time histories of the system responses for the tests performed on May 31, 2019.

mild weather and hot weather, we conclude that the impact of eco-cooling in hot weather is more pronounced than the one in mild weather. This conclusion is consistent with the observation that, in mild weather, although eco-cooling saves much more A/C system energy than in hot weather, the cooling performance is also considerably compromised.

Fig. 19 provides an example of the responses during the tests performed on May 31 when it was sunny and the ambient air temperature was 27 °C. As shown in Fig. 19(d), the eco-cooling is achieved by coordinating the A/C compressor power with vehicle speed, while, in the constant cooling case, the compressor power is relatively constant. Note that the trajectories of the average cabin temperature shown in Fig. 19(a) are similar for both cases with maximum deviation at around 1 °C. Fig. 19(b) and (c) illustrates the time history comparisons of the evaporator wall temperature and the vent air temperature, respectively. It is also worth mentioning that the difference in the auxiliary power trajectories between the eco-cooling and constant cooling cases may lead to different powertrain and power-split responses, for which we are unable to directly control in our test vehicle. The energy-saving numbers, however, are consistent with simulation results.

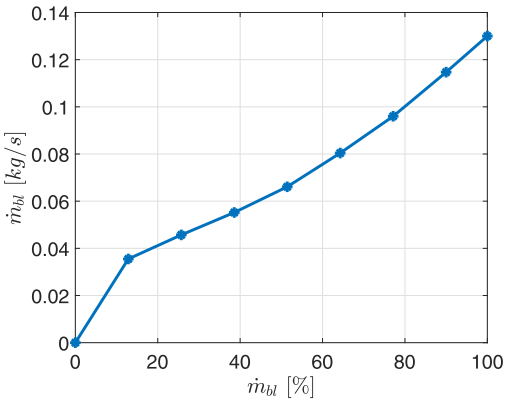

Fig. 20. HVAC blower airflow map.

1) *Remark:* One approach for deploying our strategy in production vehicles could be offering drivers/passengers with an energy-saving mode button/option, in which they obtain energy savings if they do not intervene with the A/C system settings and let the eco-cooling strategy control the A/C system autonomously.

VI. Conclusion

In this article, an eco-cooling strategy was proposed for the efficient operation of A/C systems in electrified vehicles. The eco-cooling strategy leverages the A/C system efficiency dependence on the vehicle speed and incorporates the speed preview information to capitalize on this sensitivity. The eco-cooling strategy was realized through an MPC approach and validated in closed-loop simulations with a high-fidelity simulation model of an electrified A/C system. After demonstrating the effectiveness of the proposed eco-cooling strategy on the simulation model, modifications were made so that it becomes suitable for implementation on a test HEV, i.e., 2017 Toyota Prius. Based on the repeated vehicle tests over the same real-word city driving cycle, the eco-cooling strategy was shown to be able to save, on average, 8% of the A/C system energy, which translates to 5.7% energy saving at the vehicle level, compared with the constant A/C control case (benchmark case). Key contributions can be summarized as: 1) the development of MPC-based eco-cooling strategy that allows for leveraging A/C system efficiency sensitivity to the vehicle speed and 2) the experimental validation of the eco-cooling strategy on the test vehicle.

Appendix

Fig. 20 shows the HVAC blower flow rate mapping between the percentage PWM control signal and the actual flow rate into the cabin in kg/s.

Note that this map is validated for the case with the blend door position at the front vent position and with no cabin air recirculation, which is the case for all the test results presented in this article. While the blend door position changes or the recirculation is ON, due to the back-pressure variations, the same percentage PWM control signal of the HVAC blower may result in different airflow rates into the cabin. In addition, since the calibration experiments were performed in a

well-controlled lab environment, the uncertainties associated with the ambient conditions during the open road tests, e.g., ambient temperature, pressure, and humidity, could also affect the actual airflow rate into the cabin.

REFERENCES

[1] M. H. Salah, T. H. Mitchell, J. R. Wagner, and D. M. Dawson, "Nonlinear-control strategy for advanced vehicle thermal-management systems," *IEEE Trans. Veh. Technol.*, vol. 57, no. 1, pp. 127–137, Jan. 2008.

[2] A. Y. Karnik, A. Fuxman, P. Bonkoski, M. Jankovic, and J. Pekar, "Vehicle powertrain thermal management system using model predictive control," *SAE Int. J. Mater. Manuf.*, vol. 9, no. 3, pp. 525–533, Apr. 2016.

[3] Y. Yang *et al.*, "Thermal management of electric machines," *IET Elect. Syst. Transp.*, vol. 7, no. 2, pp. 104–116, Jun. 2017.

[4] S. Bauer, A. Suchaneck, and F. P. León, "Thermal and energy battery management optimization in electric vehicles using Pontryagin's maximum principle," *J. Power Sources*, vol. 246, pp. 808–818, Jan. 2014.

[5] Y. Masoudi and N. L. Azad, "MPC-based battery thermal management controller for plug-in hybrid electric vehicles," in *Proc. Amer. Control Conf. (ACC)*, Seattle, WA, USA, May 2017, pp. 4365–4370.

[6] M. R. Amini, J. Sun, and I. Kolmanovsky, "Two-layer model predictive battery thermal and energy management optimization for connected and automated electric vehicles," in *Proc. IEEE Conf. Decis. Control (CDC)*, Dec. 2018, pp. 6976–6981.

[7] R. Cloudt and F. Willems, "Integrated emission management strategy for cost-optimal engine-aftertreatment operation," *SAE Int. J. Engines*, vol. 4, no. 1, pp. 1784–1797, Apr. 2011.

[8] H. Wang, I. Kolmanovsky, M. R. Amini, and J. Sun, "Model predictive climate control of connected and automated vehicles for improved energy efficiency," in *Proc. Annu. Amer. Control Conf. (ACC)*, Milwaukee, WI, USA, Jun. 2018, pp. 828–833.

[9] H. Wang, M. R. Amini, Z. Song, I. Kolmanovsky, and J. Sun, "Combined energy and comfort optimization of air conditioning system in connected and automated vehicles," in *Proc. ASME Dyn. Syst. Control Conf. (DSCC)*, Park City, UT, USA, Oct. 2019, p. 9.

[10] X. Yan, J. Fleming, and R. Lot, "A/C energy management and vehicle cabin thermal comfort control," *IEEE Trans. Veh. Technol.*, vol. 67, no. 11, pp. 11238–11242, Nov. 2018.

[11] J. Brusey, D. Hintea, E. Gaura, and N. Beloe, "Reinforcement learning-based thermal comfort control for vehicle cabins," *Mechatronics*, vol. 50, pp. 413–421, Apr. 2018.

[12] S. E. Shladover, "Connected and automated vehicle systems: Introduction and overview," *J. Intell. Transp. Syst.*, vol. 22, no. 3, pp. 190–200, May 2018.

[13] A. Vahidi and A. Sciarretta, "Energy saving potentials of connected and automated vehicles," *Transp. Res. C, Emerg. Technol.*, vol. 95, pp. 822–843, Oct. 2018.

[14] J. Guanetti, Y. Kim, and F. Borrelli, "Control of connected and automated vehicles: State of the art and future challenges," *Annu. Rev. Control*, vol. 45, pp. 18–40, Jan. 2018.

[15] X. Gong, H. Wang, M. R. Amini, I. Kolmanovsky, and J. Sun, "Integrated optimization of power split, engine thermal management, and cabin heating for hybrid electric vehicles," in *Proc. 3rd IEEE Conf. Control Technol. Appl. (CCTA)*, Hong Kong, Aug. 2019, pp. 567–572.

[16] M. R. Amini, X. Gong, Y. Feng, H. Wang, I. Kolmanovsky, and J. Sun, "Sequential optimization of speed, thermal load, and power split in connected HEVs," in *Proc. Amer. Control Conf. (ACC)*, Philadelphia, PA, USA, Jul. 2019, pp. 4614–4620.

[17] M. R. Amini, H. Wang, X. Gong, D. Liao-McPherson, I. Kolmanovsky, and J. Sun, "Cabin and battery thermal management of connected and automated HEVs for improved energy efficiency using hierarchical model predictive control," *IEEE Trans. Control Syst. Technol.*, vol. 28, no. 5, pp. 1711–1726, Sep. 2020.

[18] J. Rugh and R. Farrington, "Vehicle ancillary load reduction project close-out report: An overview of the task and a compilation of the research results," Nat. Renew. Energy Lab. (NREL), Golden, CO, USA, Tech. Rep. NREL/TP-540-42454, 2008.

[19] M. Jeffers, L. Chaney, and J. Rugh, "Climate control load reduction strategies for electric drive vehicles in warm weather," SAE Tech. Paper 2015-01-0355, 2015.

[20] (Jun. 2014). *NREL Works to Increase Electric Vehicle Efficiency Through Enhanced Thermal Management*. [Online]. Available: https://www.nrel.gov/docs/fy14osti/62241.pdf

[21] T. Kiss, L. Chaney, and J. Meyer, "New automotive air conditioning system simulation tool developed in MATLAB/simulink," SAE Tech. Paper 2013-01-0850, 2013.

[22] Q. Zhang, Y. Meng, C. Greiner, C. Soto, W. Schwartz, and M. Jennings, "Air conditioning system performance and vehicle fuel economy trade-offs for a hybrid electric vehicle," SAE Tech. Paper 2017-01-0171, Mar. 2017.

[23] H. Wang *et al.*, "MPC-based precision cooling strategy (PCS) for efficient thermal management of automotive air conditioning system," in *Proc. 3rd IEEE Conf. Control Technol. Appl. (CCTA)*, Hong Kong, Aug. 2019, pp. 573–578.

[24] Q. Zhang, S. E. Li, and K. Deng, *Automotive Air Conditioning: Optimization, Control and Diagnosis*. Cham, Switzerland: Springer, 2016.

[25] M. Risbeck and J. Rawlings, "MPCTools: Nonlinear model predictive control tools for CasADi," Tech. Rep., 2016. [Online]. Available: https://sites.engineering.ucsb.edu/~jbraw/software/mpctools/index.html

[26] J. A. E. Andersson, J. Gillis, G. Horn, J. B. Rawlings, and M. Diehl, "CasADi: A software framework for nonlinear optimization and optimal control," *Math. Program. Comput.*, vol. 11, no. 1, pp. 1–36, Mar. 2019.

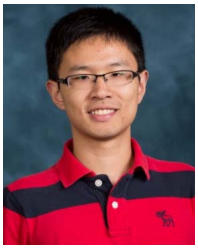

Hao Wang received the B.E. degree in vehicle engineering from the Hefei University of Technology, Hefei, China, in 2012, and the M.S.E. degree in mechanical engineering and the Ph.D. degree in naval architecture and marine engineering from the University of Michigan, Ann Arbor, MI, USA, in 2014 and 2019, respectively.

His research interests include set-membership identification and its applications, energy optimization of connected vehicles, and optimal control of electrified powertrain systems.

Mohammad Reza Amini (Member, IEEE) received the Ph.D. degree in mechanical engineering from Michigan Tech University, Houghton, MI, USA, in 2017.

He is currently an Assistant Research Scientist with the College of Engineering, University of Michigan, Ann Arbor, MI, USA. His research interests in nonlinear, adaptive, and predictive control theories and their applications to intelligent transportation, automotive, and energy systems.

Qiuhao Hu received the bachelor's degree in naval architecture and ocean engineering and the master's degree in naval architecture and ocean engineering from Shanghai Jiao Tong University, Shanghai, China, in 2015 and 2018, respectively. He is currently pursuing the Ph.D. degree with the Department of Naval Architecture and Marine Engineering, University of Michigan, Ann Arbor, MI, USA.

His research interests are in the hybrid electric system, thermal and power management, adaptive control, and optimal control.

Ilya Kolmanovsky (Fellow, IEEE) received the M.S. and Ph.D. degrees in aerospace engineering and the M.A. degree in mathematics from the University of Michigan, Ann Arbor, MI, USA, in 1993, 1995, and 1995, respectively.

He is currently a Full Professor with the Department of Aerospace Engineering, University of Michigan, with research interests in control theory for systems with state and control constraints and in control applications to automotive and aerospace systems. Before joining the University of Michigan as a Faculty Member, he has been with Ford Research and Advanced Engineering, Dearborn, MI, USA, for close to 15 years, where the focus of his research has been on advanced control of engines and powertrain systems to improve their energy efficiency, emissions, and performance.

Dr. Kolmanovsky was a recipient of the Donald P. Eckman Award of the American Automatic Control Council, two IEEE TRANSACTIONS ON CONTROL SYSTEMS TECHNOLOGY Outstanding Paper Awards, and several awards from Ford Research and Advanced Engineering. He is also named an Inventor on 98 United States Patents.

Jing Sun (Fellow, IEEE) received the B.S. and M.S. degrees from the University of Science and Technology of China, Hefei, China, in 1982 and 1984, respectively, and the Ph.D. degree from the University of Southern California, Los Angeles, CA, USA, in 1989.

From 1989 to 1993, she was an Assistant Professor with the Electrical and Computer Engineering Department, Wayne State University, Detroit, MI, USA. She joined the Ford Research Laboratory, Dearborn, MI, in 1993, where she was with the Powertrain Control Systems Department. After spending almost ten years in the industry, she came back to academia and joined the faculty of the College of Engineering, University of Michigan, Ann Arbor, MI, in 2003, where she is currently the Michael G. Parsons Professor and the Chair of the Department of Naval Architecture and Marine Engineering, with courtesy appointments as a Professor with the Department of Electrical Engineering and Computer Science and the Department of Mechanical Engineering. She has coauthored a textbook on robust adaptive control. She holds 39 U.S. patents. Her research interest includes system and control theory and its applications to marine and automotive propulsion systems.

Dr. Sun was a recipient of the 2003 IEEE Control System Technology Award.